












Article

Synthesis, Anti-Inflammatory Activity, and Docking Simulation of a Novel Styryl Quinolinium Derivative

Mina Todorova ¹, Romyana Bakalska ¹, Mehran Feizi-Dehnaeybi ², Ghodsi Mohammadi Ziarani ², Mina Pencheva ³, Kirila Stojnova ⁴, Miglena Milusheva ^{1,5}, Paraskev Nedialkov ⁶, Emiliya Cherneva ^{7,8}, Tsonko Kolev ⁹ and Stoyanka Nikolova ^{1,*}

- ¹ Department of Organic Chemistry, Faculty of Chemistry, University of Plovdiv, 4000 Plovdiv, Bulgaria; minatodorova@uni-plovdiv.bg (M.T.); bakalska@uni-plovdiv.bg (R.B.); miglena.milusheva@uni-plovdiv.bg or miglena.milusheva@mu-plovdiv.bg (M.M.)
- ² Department of Organic Chemistry, Faculty of Chemistry, Alzahra University, Tehran 19938-93973, Iran; m.feizi@alzahra.ac.ir (M.F.-D.); gmohammadi@alzahra.ac.ir (G.M.Z.)
- ³ Department of Medical Physics and Biophysics, Faculty of Pharmacy, Medical University of Plovdiv, 4002 Plovdiv, Bulgaria; mina.pencheva@mu-plovdiv.bg
- ⁴ Department of General and Inorganic Chemistry with Methodology of Chemistry Education, Faculty of Chemistry, University of Plovdiv, 4000 Plovdiv, Bulgaria; stojnova@uni-plovdiv.bg
- ⁵ Department of Bioorganic Chemistry, Faculty of Pharmacy, Medical University of Plovdiv, 4002 Plovdiv, Bulgaria
- ⁶ Department of Pharmacognosy, Faculty of Pharmacy, Medical University of Sofia, 1000 Sofia, Bulgaria; pnedialkov@pharmfac.mu-sofia.bg
- ⁷ Department of Chemistry, Faculty of Pharmacy, Medical University of Sofia, 2 Dunav Str., 1000 Sofia, Bulgaria; cherneva@pharmfac.mu-sofia.bg
- ⁸ Institute of Organic Chemistry with Centre of Phytochemistry, Bulgarian Academy of Sciences, Acad. G. Bonchev Str., build. 9, 1113 Sofia, Bulgaria
- ⁹ Institute of Molecular Biology "R. Tsanev", Bulgarian Academy of Sciences, Acad. G. Bonchev Str, bl. 21, 1113 Sofia, Bulgaria; tskolev@bio21.bas.bg
- * Correspondence: tanya@uni-plovdiv.bg



Academic Editor: Gang Wei

Received: 2 December 2024

Revised: 20 December 2024

Accepted: 25 December 2024

Published: 31 December 2024

Citation: Todorova, M.; Bakalska, R.; Feizi-Dehnaeybi, M.; Ziarani, G.M.; Pencheva, M.; Stojnova, K.; Milusheva, M.; Nedialkov, P.; Cherneva, E.; Kolev, T.; et al. Synthesis, Anti-Inflammatory Activity, and Docking Simulation of a Novel Styryl Quinolinium Derivative. *Appl. Sci.* **2025**, *15*, 284. <https://doi.org/10.3390/app15010284>

Copyright: © 2024 by the authors. Licensee MDPI, Basel, Switzerland. This article is an open access article distributed under the terms and conditions of the Creative Commons Attribution (CC BY) license (<https://creativecommons.org/licenses/by/4.0/>).

Abstract: Stilbenes, like resveratrol, are natural small molecules with several applications in the treatment of chronic illnesses, diabetes, and neurological and cardiovascular conditions. Considering the molecular structure of stilbenes and the biological activities of resveratrol, we investigated the synthesis and biological activity of a novel styryl quinolinium (SQ) derivative. The SQ was synthesized using the alkylation of lepidine and methyl 4-methylbenzenesulfonate and further Knoevenagel condensation with 2-hydroxy naphthaldehyde. Its structure was determined using NMR, IR, Raman, UV-Vis, and MS. The current trend of research has shifted toward the synthesis of novel SQ as resveratrol's analog. Therefore, its anti-inflammatory and antioxidant activities were evaluated. The compound exerted very good anti-inflammatory effects in preventing albumin denaturation, which were confirmed by ex vivo immunohistochemical studies. Density functional theory (DFT) analyses were conducted on the SQ structure to gain detailed insights into its active sites, energy gap, quantum properties, and electronic behavior. The biological evaluation of the compound was completed, assessing its antioxidant potential using DPPH radical scavenging assay. In addition, molecular docking simulations were utilized to assess the SQ compound's potential inhibitory effect on human serum albumin (HSA).

Keywords: styryl quinolinium; synthesis; in silico; anti-inflammatory; albumin denaturation; immunohistochemical analysis; antioxidant activity; docking

1. Introduction

Inflammation is a dynamic reaction of the body to an external factor that disrupts its natural balance, usually pathogenic microbes or physical agents. This procedure most often helps to eliminate the cause of tissue damage, but in other diseases, the body's response is insufficient. Prolonged inflammation may cause tissue damage, cellular destruction, or even accelerate the development of cancer [1]. In addition to discomfort, heat, and loss of function, localized redness and swelling are the most common first signs of inflammation [2]. These outcomes originate from the body's response to inflammatory agents, which start a cascade of events that include many inflammatory mediators, such as proinflammatory cytokines IL-1 or TNF- α , anti-inflammatory cytokines IL-10 or IL-13, etc. [3,4]. These mediators are some of the potential key targets in the search for novel anti-inflammatory drugs.

Stilbenes (Figure 1), as natural small molecules, are used in the treatment of chronic disorders such as diabetes, as well as neurological and cardiovascular conditions [5,6]. Their significance as anticancer agents is very important. Resveratrol (3,5,4'-trihydroxy-trans-stilbene), for example, is a polyphenol, having two phenol rings joined by an ethylene bridge. It is a naturally occurring compound that is beneficial for age-related diseases, such as oxidative stress, neurodegeneration, inflammation, diabetes, and cardiovascular diseases. The antioxidative properties of resveratrol and its analogs have attracted significant attention because they block reactive oxygen species, which are linked to oxidative stress [7,8]. Resveratrol has a wide spectrum of biological activities, but its low water solubility, instability, and low bioavailability have limited its widespread application in pharmaceuticals, foods, and cosmetics [9–17].

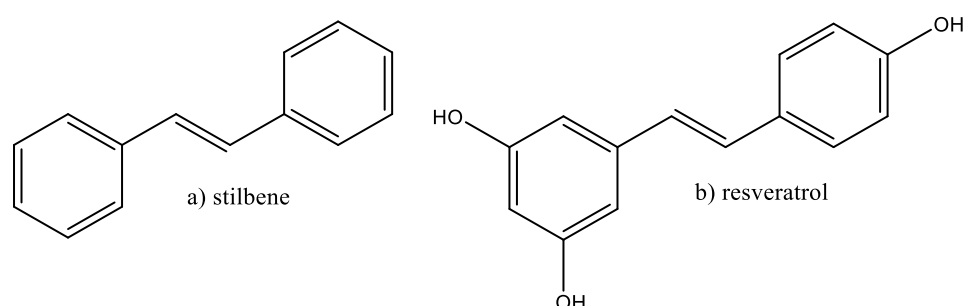


Figure 1. Structures of stilbene (a) and resveratrol (b).

Sulfonate-based compounds, on the other hand, have been reported to inhibit the activities of cyclooxygenases (COXs) and acetylcholinesterase (AChE) activities [18]. They can enhance the physicochemical characteristics of the drug molecules by generating relatively strong hydrogen bonding and electrostatic interactions with protein residues in the receptor binding site [19,20].

Considering the molecular structure of stilbenes and the biological activities of its derivative resveratrol, we investigated the substitution of the resorcinol ring with a naphthol one in order to promote the formation of intramolecular hydrogen bonds between OH with the sulphonyl group, as well as that of the phenol ring with quinolinium and how that substitution would affect the anti-inflammatory and antioxidant potential of the resulting compound.

2. Materials and Methods

2.1. Chemicals

All solvents and reagents were purchased from Aldrich (Merck KGaA, Darmstadt, Germany). The melting point was determined on a DSC. The compound was characterized

using different techniques. The purity of the SQ was determined by TLC, which was carried out on precoated 0.2 mm Merck silica gel 60 plates (Merck KGaA, Darmstadt, Germany), using hexane:ethyl acetate = 1:2, petroleum ether:diethyl ether = 2:1, and n-propanol:formic acid = 8:2 as chromatographic systems.

2.2. Measurements

The UV–visible spectra were recorded on a Cary-60 (Agilent Technologies, Santa Clara, CA, USA) and the fluorescence spectra on a Hitachi F-2700 spectrometer (Hitachi High-Tech Science Corp., Tokyo, Japan) ranging from 500 to 900 nm in four solvents (water, methanol, acetonitrile, and chloroform), at a concentration of 1×10^{-5} M. The IR spectra were determined on a VERTEX 70 FT-IR spectrometer (Bruker Optics, Ettlingen, Germany) in KBr tablets, ranging from 4000 to 400 cm^{-1} , 2 cm^{-1} resolution ability, 25 scans.

The NMR spectra were recorded at room temperature at 500 MHz on a Bruker Avance III HD 500 spectrometer (Bruker, Billerica, MA, USA).

A Differential Scanning Calorimeter, Phoenix DSC 204 F1 (Netzsch-Gerätebau GmbH, Selb, Germany), was applied to carry out the thermal analysis. The experiment was conducted under argon atmosphere (scanning rate—10 $^{\circ}\text{C}/\text{min}$, cooling 40 $^{\circ}\text{C}/\text{min}$).

The chromatographic system Thermo Dionex Ultimate 3000 LC and the triple-quadrupole mass spectrometer Thermo TSQ Quantum Access MAX (Thermo Fisher Scientific, Waltham, MA, USA) with Heated Electrospray Ionization (HESI) were used to perform liquid chromatography with mass detection (LC-MS/MS) of analytes. The chromatographic separation was carried out on an AccucoreTM RP-MS (Thermo Fisher Scientific, Waltham, MA, USA) core-shell analytical column (100 mm length, 2.1 mm diameter, 2.6 μm particles) under isocratic conditions.

The peak shapes and MS signals of the analytes were improved by using mobile phases A: 0.1% formic acid in acetonitrile–water (90:10, v/v); and B: 0.1% formic acid in acetonitrile–water (10:90, v/v) in 40:60 (A:B) ratio at flow rate of 0.150 mL min^{-1} . HESI was used for analyte detection in positive ionization mode with spray voltage –4000 V; source temperature 400 $^{\circ}\text{C}$; sheath gas pressure 30; vaporizer temperature 350 $^{\circ}\text{C}$; and capillary temperature 270 $^{\circ}\text{C}$. Protonated molecules of the analyte were used as precursor ions for selected reaction monitoring (SRM).

2.3. Synthetic Methods: Experimental Protocols and Spectral Data

2.3.1. Synthesis of Lepidine Methyl Tosylate

To a solution of lepidine (**1**) (1.0800 g, 7.5 mmol) in dry toluene (20 mL), methyl 4-methylbenzenesulfonate (methyl tosylate) (**2**) (2.4800 g, 7.5 mmol) was added. The quaternary salt was obtained in 14 h reflux. The resulting crystals were filtered and washed with toluene to remove unreacted lepidine and dried over P_2O_5 at room temperature, with a yield of 84%.

IR [KBr]: $\nu[\text{cm}^{-1}]$ 2919, 1620, 1607, 1591, 1531, 1494, 1442, 1402, 1384, 1369, 1348, 1267, 1220, 1191, 1117, 1033, 963, 828, 772.

The obtained salt was applied directly for the synthesis of SQ.

2.3.2. Synthesis of SQ (**5**) (E)-4-(2-(2-Hydroxynaphthalen-1-yl)vinyl)-1-methylquinolin-1-ium 4-Methylbenzenesulfonate

Lepidine methyl tosylate (**3**) (0.50 g, 1.5 mmol) and 2-hydroxynaphthaldehyde (**4**) (0.26 g, 1.5 mmol) were dissolved in 20 mL of dry benzene. Piperidine (0.01 g, 0.15 mmol), glacial acetic acid (0.02 g, 0.3 mmol), and 5 mL of dimethylformamide were added, and the reaction mixture was refluxed for 28 h (Warning: Benzene can cause cancer or birth defects!). Then, the crystals were filtered off, washed with benzene, dried at room temperature, and

recrystallized from methanol. The yield of orange needle crystals was 71.4%, with a melting point of 252.6 °C (DSC) (Figure 2).

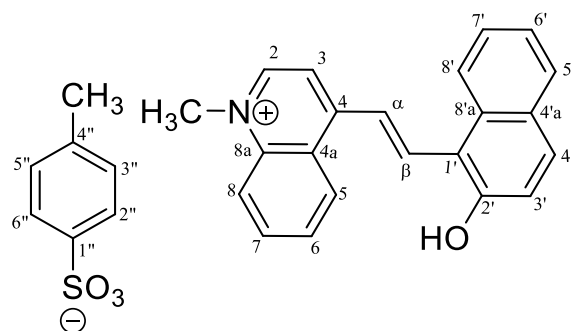


Figure 2. Structural formula of SQ (5) with the number of atoms used in the assignment of signals in NMR.

^1H NMR: 11.12 (broad s, 1H, naphthol OH), 9.27 (d, $J = 6.5$, 1H, quinolinium H2), 8.66 (d, $J = 6.5$, 1H, quinolinium H3), 8.63 (d, $J = 8.4$, 1H, quinolinium H5), 8.59 (s, 2H, $\text{H}\alpha$, $\text{H}\beta$), 8.46–8.38 (m, $J = 8.4$, 7.7, 2H, quinolinium H8, naphthol H8'), 8.23 (m, 1H, quinolinium H7), 8.02 (t, $J = 7.7$, 1H, quinolinium H6), 7.90 (d, $J = 8.9$, 1H, naphthol H5'), 7.87 (d, $J = 7.5$, 1H, naphthol H4'), 7.58 (ddd, $J = 8.4$, 6.9, 1.2, 1H, naphthol H7'), 7.51 (d, $J = 8.1$, 2H, tosylate H2'', H6''), 7.41 (t, $J = 7.4$, 1H, naphthol H6'), 7.35 (d, $J = 8.9$, 1H, naphthol H3'), 7.10 (d, $J = 7.9$, 2H, Ar, tosylate H3'', H5''), 4.54 (s, 3H, quinolinium N-CH₃), 2.26 (s, 3H, CH₃ tosylate).

^{13}C NMR: 157.24 (naphthol C2'), 153.92 (quinolinium C4), 148.32 (quinolinium C2), 146.14 (tosylate C1''), 139.11 (quinolinium C8a), 138.12 (tosylate C4''), 136.74 (C β), 135.21 (quinolinium C7), 133.30 (naphthol C8'a), 132.92 (naphthol C5'), 129.88 (quinolinium C6), 129.24 (naphthol C4'), 128.55 (naphthol C4'a), 128.53 (tosylate C3'', C5''), 127.99 (naphthol C7'), 126.55 (quinolinium C4a), 126.01 (quinolinium C5), 125.96 (tosylate C2'', C6''), 123.92 (naphthol C6'), 123.80 (C α), 123.32 (naphthol C8'), 119.88 (quinolinium C8), 119.00 (naphthol C3'), 116.58 (quinolinium C3), 114.57 (naphthol C1'), 44.97 (quinolinium N-CH₃), 21.23 (tosylate CH₃).

HESI, m/z calculated for $\text{C}_{22}\text{H}_{18}\text{NO}^+ = 312.384$, found 312.142 (mass error 2.42 ppm).

2.4. In Silico Pharmacokinetic Profiling and Toxicity Analysis

2.4.1. Theoretical Prediction of Pharmacokinetic Parameters (ADME)

The physicochemical and pharmacokinetic parameters, as well as drug-likeness of the compound, were analyzed using the SwissADME free web tool (accessed on 21 October 2024) [21].

2.4.2. Theoretical Prediction of Toxicity

The ProTox-II free web tool (accessed on 11 October 2024) was used to predict toxicity class and LD₅₀ for the compound [22,23].

2.4.3. PASS Online Predictions

The computer-based PASS Online free web tool (accessed on 19 September 2024) was used to predict the biological activities of the compound [24–26].

2.5. In Vitro Inhibition of Albumin Denaturation

The antidenaturation assay was carried out in accordance with Milusheva et al.'s method [26]. The reaction mixture contained 0.2 mL of the tested drug dissolved in DMSO (0.5 mg/mL) and 0.5 mL of a 5% aqueous solution of human albumin (Albumorm 20, Octapharma (IP) SPRL, 1070 Anderlecht, Belgium). For 15 min, the samples were incubated

at 37 °C. Subsequently, each tube was filled with 2.5 mL of phosphate-buffered saline (pH 6.3), and the samples were heated at 80 °C for 30 min before being cooled for 5 min. The turbidity was measured at 660 nm spectrophotometrically (Cary 60 UV-Vis, Agilent Technologies, Santa Clara, CA, USA). For the blank sample, a mixture of 2.5 mL of buffer and 0.2 mL of DMSO was used instead of the compounds, while the product control test lacked the compounds, having 0.5 mL of serum albumin and 2.5 mL of buffer only. The percentage of inhibition of protein denaturation was calculated as follows:

$$\text{Percentage of inhibition denaturation} = [(\text{Absorbancecontrol} - \text{Absorbancesample}) / \text{Absorbancecontrol}] \times 100$$

The control represents 100% protein denaturation. The commercially available anti-inflammatory drugs diclofenac and acetylsalicylic acid (ASA) were used for comparison. Their anti-inflammatory effect was determined as a percentage of inhibition of albumin denaturation, following the same protocol as for the novel compounds.

2.6. *Ex Vivo* Immunohistochemical Methods

2.6.1. Animals, Tissues, and Preparations

Eight Wistar rats (270 ± 15 g body weight, male, 11 weeks age) were purchased from the Medical University of Plovdiv Animal Laboratory, Bulgaria. The experimental procedures were conducted according to the previously described protocol [26,27].

2.6.2. Histology and Immunohistochemistry

The morphometric analysis involved tissue slices 5 µm in thickness, obtained from the circular and longitudinal layer of SM cells, as well as in the myenteric plexus of the stomach. The intensity of the immune reaction in the stomach was measured in arbitrary units (AU) on the slices immunostained for IL-1β and nNOS. The measurements were performed using the DP-Soft ver. 3.2 software, Olympus, Japan. The average intensity of pixels was recorded in arbitrary units in the range of 0–256 on microphotographs of the stomach, 0 being black and 256 being white. A minimum of 50 points were measured in the stomach at a magnification of $\times 400$. All measurements involved five slices per animal and an examination of all cross-sections of the stomach.

Paraffin sections of 5 µm thickness were subjected to hematoxylin and eosin (H-E) staining for the histochemical analysis. For all samples, immunostaining was performed through a fully automated and standardized procedure, using an Autostainer Link 48 (Dako, Agilent Technologies Inc., Glostrup, Denmark). The paraffin sections were treated for 20 min with an EnVision FLEX Visualization System (Dako, Agilent Technologies Inc., Glostrup, Denmark). Endogenous peroxidase was blocked with 3% hydrogen peroxide for 5 min. Then, the sections were incubated for 30 min with the IL-1β primary antibody (E-AB-52153; Elabscience Biotechnology Inc., Houston, TX, USA). The EnVision FLEX Visualization System containing 3,3-diamino-benzidine dihydrochloride and hematoxylin were used for visualization. The stained sections were permanently mounted with Canada balsam.

2.7. Ethics Statement

The experiments were approved by the Ethical Committee of the Bulgarian Food Agency with permit No. 229/09.04.2019 and were carried out following the guidelines of European Directive 2010/63/EU. The animals were provided by the Medical University of Plovdiv (Animal House, Plovdiv, Bulgaria).

2.8. DPPH Free-Radical Scavenging Assay

The DPPH free-radical scavenging activity was measured as reported in [28]: 0.12 mM DPPH was dissolved in methanol. The absorbance change was measured at 515 nm on a UV-Vis spectrophotometer (Cary 60 UV-Vis, Agilent Technologies, Santa Clara, CA, USA) within 30 min. The total DPPH radical scavenging activity within 30 min was measured in triplicate. The blank sample was prepared as above by replacing the test sample with equivalent methanol. The IC₅₀ value determined the effective concentration at which 50% of DPPH radicals were scavenged. A lower IC₅₀ value indicated a higher antioxidant activity.

2.9. Statistical Analysis

For the analysis of variance, the InStat computer program was utilized. Each group's mean and standard error of mean were determined. To compare various groups with their corresponding controls for repeated measurements, a two-way ANOVA was employed. A significant difference was deemed to be represented by a *p*-value of less than 0.05. The statistical software IBM SPSS Statistics v. 26 was utilized for the analyses.

2.10. DFT Investigations

The molecular structure of the SQ compound was drawn using GaussView 6, with comprehensive optimization performed through Gaussian 09W software [29]. To ensure precision, the computational approach applied density functional theory (DFT) using the B3LYP functional alongside the 6-311g (d,p) basis set, allowing the structures to remain entirely unrestricted. A frequency analysis was integrated into the optimization, confirming that each vibrational frequency displayed a positive value and affirming their positions as true minima on the potential energy landscape. Further analyses at the DFT/B3LYP/6-311g (d,p) level provided valuable insights into various properties of the compounds. These analyses included mapping the molecular electrostatic potential (MEP) surfaces, determining the energy levels of the highest occupied molecular orbital (HOMO) and the lowest unoccupied molecular orbital (LUMO), and calculating the quantum chemical reactivity descriptors, which together offer a deeper understanding of the compounds' electronic structure and reactivity.

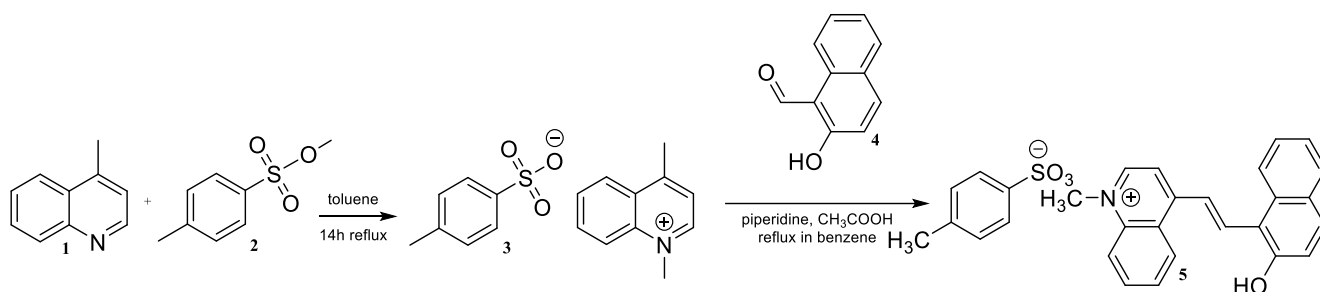
2.11. Molecular Docking Simulation

A docking simulation is an essential tool for exploring how newly synthesized compounds interact with proteins, making it invaluable for drug design and development. In this study, molecular docking simulations were carried out to assess the inhibitory effects of the SQ compound against human serum albumin (HSA), utilizing AutoDock 4.2 [30] and AutoDock Tools 1.5.6 [31]. This approach allowed for a detailed analysis of the binding affinities and interaction modes between the compound and HSA, as well as an examination of their potential anticoagulant properties. The X-ray crystal structure of HSA (PDB ID: 2I2Z) was sourced from the Protein Data Bank, while the structure of the synthesized compound was modeled using DFT calculations. The protein preparation followed the protocols established in previous research [32]. The docking was conducted with a 3D grid size of 60 × 70 × 60 Å across both HSA binding sites, using a spacing parameter of 0.375 Å, while other docking parameters remained at their default settings. The visualization of docking sites and interaction diagrams was achieved with Discovery Studio 4.1 software, providing a clear depiction of the binding interactions.

3. Results and Discussion

3.1. Synthesis, Spectral, and Structural Analysis of Styryl Quinolinium (SQ)

N-alkyl quaternary ammonium compounds are commonly used as precursors for photochromic spiropyrans [33], various cyanine dyes [34], and RNA antagonists [35]. Here, we describe the two-step synthesis of SQ as follows: (1) 4-methylquinoline (lepidine) (**1**) is alkylated with methyl toluenesulfonate (**2**) to get the quaternary salt (**3**); and (2) the resulting lepidinium salt (**3**) is then applied in Knoevenagel condensation with 2-hydroxy naphthaldehyde (**4**) (Scheme 1). Dry toluene was used to alkylate equimolar quantities of lepidine and methyl 4-methylbenzenesulfonate. The solvent was chosen due to the easiness of crystallization and separation of the product. Lepidine has a very good solubility in toluene, but lepidinium methyl tosylate as a salt does not dissolve in toluene. Thus, the quaternary salt was obtained in 84% yield. The obtained salt (**3**) then was directly applied in Knoevenagel condensation with 2-hydroxy naphthaldehyde (**4**) to the SQ (**5**) formation. The SQ salt was obtained in high purity and yield.



Scheme 1. Synthesis of SQ (**5**).

The obtained SQ (**5**) was slightly soluble in non-polar and well soluble in polar organic solvents. The emission spectra of SQ in four solvents—water, methanol, acetonitrile, and chloroform—were measured. The comparative ultraviolet–visible and fluorescent spectra of the SQ (**5**) under study at the same concentration of the solutions are shown in Figure S1 (Supplementary Materials Figure S1).

The fluorescence spectra in the solvents chloroform, acetonitrile, and methanol were normal with a maximum in the range of 595–615 nm (Figure S1B) and were a mirror image of their absorption spectra (Figure S1A). This normality implies that the molecule was behaving consistently across these solvents, and there were no unexpected solvent-dependent changes or anomalies. In the polar water solvent, the emission spectrum had a discrete structure. When the emission spectrum has a discrete structure, it displays distinct, sharp lines or peaks instead of a wide, continuous band. This happens because the polar environment influences the electronic states of the dissolved molecules. Therefore, the solvent molecules stabilize certain electronic states of the solute. The calculated Stokes offset according to the type of solvent used was from 126 nm to 156 nm. The infrared spectra of SQ (**5**) offer the opportunity to study solid-phase effects, such as Evans' holes and Davydov's splitting of salt-like bands [36].

It is characteristic of the IR spectra of charge-transfer compounds that almost all oscillations are mixed. The reason for this phenomenon is that the charge in the cationic part of the SQ is strongly delocalized, as a result of which an electronic and vibrational interaction occurs. The result of this interaction is a significant shift of the bands belonging to the corresponding normal oscillations to the lower wavenumbers and an increase in the intensity of some of them [37,38]. The IR and Raman spectra of SQ (**5**) are shown in Figure S2 (Supplementary Materials Figure S2). The NMR data of **5** are presented in Figures S3–S8 (Supplementary Materials Figures S3–S8). The methine protons of the styryl double bond of

the compound resonate as a singlet for 2H at 8.59 ppm among the aromatic proton signals. The probable reason is the deviation of the two aromatic cores from the plane of the double bond. The MS spectra are presented in Figure S9 (Supplementary Materials Figure S9).

3.2. DFT Investigations

3.2.1. Molecular Geometry

The structure of the SQ compound (**5**) was optimized using DFT at the B3LYP/6-311g (d,p) computational level (Figure 3). This configuration represents the compound in its lowest energy, most stable state. The optimized geometry yields an electronic energy of -1873.70 Hartree. Additionally, the compound displays a notable dipole moment of 16.93 Debye, indicating a strong presence of dipole–dipole interactions within the SQ compound.

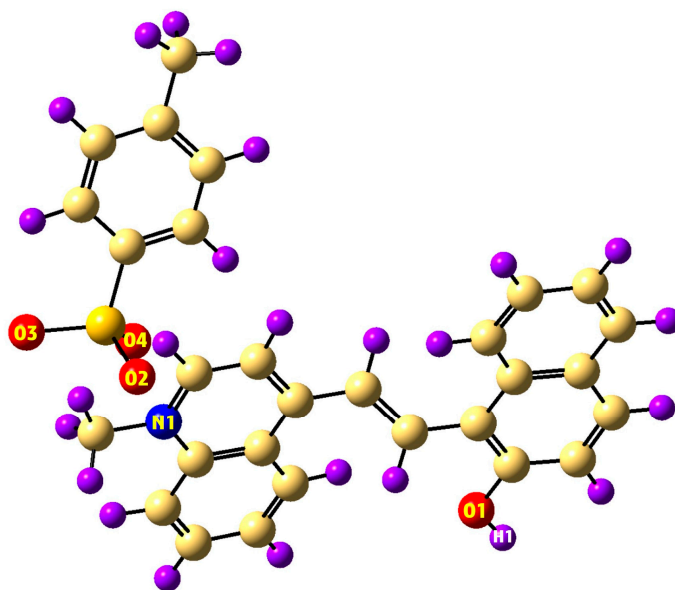


Figure 3. The proposed SQ (**5**) geometry applying the DFT/B3LYP/6-311g (d,p) level.

3.2.2. MEP Map

The molecular electrostatic potential (MEP) offers a vivid depiction of a molecule's electrostatic properties, projecting its potential energy onto a surface defined by constant electron density. This mapping allows us to visualize essential features of the molecule, such as its size, shape, and specific electrostatic potential values. MEP provides insights into key molecular characteristics like dipole moments, electronegativity, partial charges, and reactive sites, making it an invaluable tool for interpreting a molecule's polarity. The regions with negative electrostatic potential indicate areas where the molecule's concentrated electron density attracts protons, while the positive regions highlight areas where proton repulsion occurs due to a lower electron density and insufficient shielding of nuclear charges. By examining this contrast, MEP illustrates the distribution of electron density and its influence on molecular interactions. The electron density isosurface, a critical concept here, is essentially a boundary on which the molecule's electron density has a specific value, enclosing a defined fraction of its electron probability density. This surface aids in accurately representing the molecule's spatial electron distribution, thereby enhancing our understanding of its chemical behavior and reactivity [39,40]. In this visualization, a gradient of colors represents the electrostatic potential across molecular surfaces. Each color corresponds to distinct regions: red, orange, yellow, green, and blue, with a progression that reflects the increasing potential. Specifically, the red areas denote zones of maximum negative potential, while the blue regions highlight areas of maximum positive potential.

At the midpoint, green indicates areas of neutral or zero potential [41]. This color-coded approach offers a clear, intuitive way to understand the distribution of electrostatic forces within a molecule, aiding in the analysis of its chemical properties and interactions. The blue-colored regions on the surface imply an electrostatic potential that supports nucleophilic reactions, while the red areas highlight a favorable environment for electrophilic reactions [42]. To identify potential reactive sites for both electrophilic and nucleophilic attacks in the SQ (5), the MEP surface was generated based on its optimized geometry. This map was achieved using the B3LYP/6-311g (d,p) computational method, and the resulting MEP distribution is shown in Figure 4. In the SQ compound, a red-colored surface surrounds the O1, O2, and O3 atoms, highlighting their vulnerability to electrophilic attack. In contrast, a blue region appears around the H1 atom, signaling its potential for nucleophilic interaction.

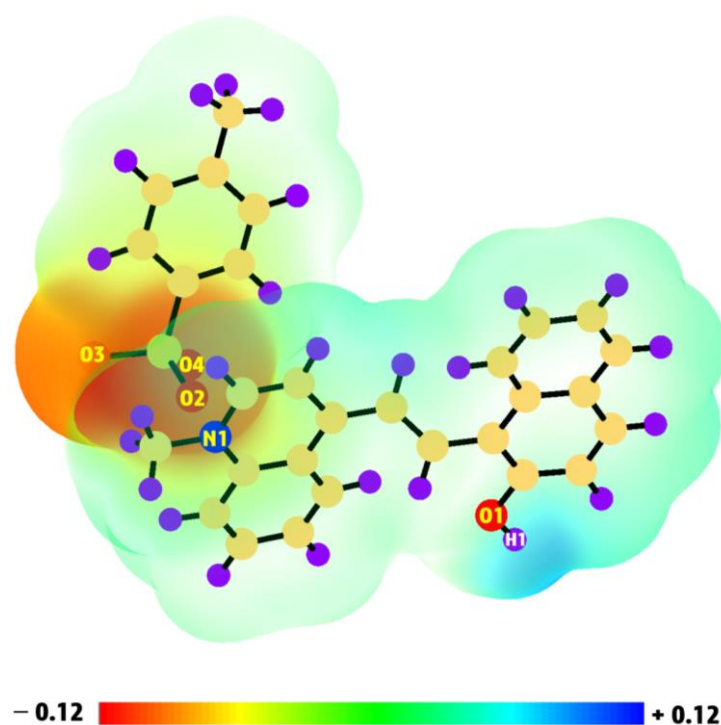


Figure 4. The MEP map of SQ (5) applying the DFT/B3LYP/6-311g (d,p) level.

3.2.3. HOMO and LUMO Molecular Orbitals and Reactivity

The analysis of frontier molecular orbitals (FMOs), specifically the HOMO and LUMO, provides valuable insights into a compound's chemical reactivity, stability, biological activity, optical features, and electronic behavior [43]. The LUMO is associated with an electron's acceptance, while the HOMO signifies electron donation. Figure 5 presents the HOMO-1, HOMO, LUMO, and LUMO + 1 contributions for the SQ compound, highlighting the calculated values of $E_{\text{HOMO-1}}$, E_{HOMO} , E_{LUMO} , and $E_{\text{LUMO+1}}$ and the energy gaps (ΔE), determined using the DFT method at the B3LYP/6-311g (d,p) level. A crucial parameter in understanding a compound's stability, reactivity, and potential biological effects is the HOMO-LUMO energy gap. Molecules with smaller energy gaps typically exhibit higher biological activity and chemical reactivity but lower stability than those with larger gaps [44]. In the SQ compound, the HOMO-LUMO analysis reveals that the electron density in the HOMO is concentrated primarily on the anionic SO_3^- group, while the LUMO's electron density is distributed across the cationic regions, suggesting an electron transfer pathway from the SO_3^- group to the cationic portions of the molecule. For SQ, the energy gap is calculated to be 1.87 eV, which is relatively low and implies enhanced reactivity and

biological activity. This narrow HOMO-LUMO gap indicates that the HOMO and LUMO energy levels are close, allowing for easy excitation of outer-layer electrons, which supports the compound's pronounced chemical and biological activity. Furthermore, the energy gap between HOMO-1 (−5.35 eV) and LUMO + 1 (−1.99 eV) is determined at 3.36 eV.

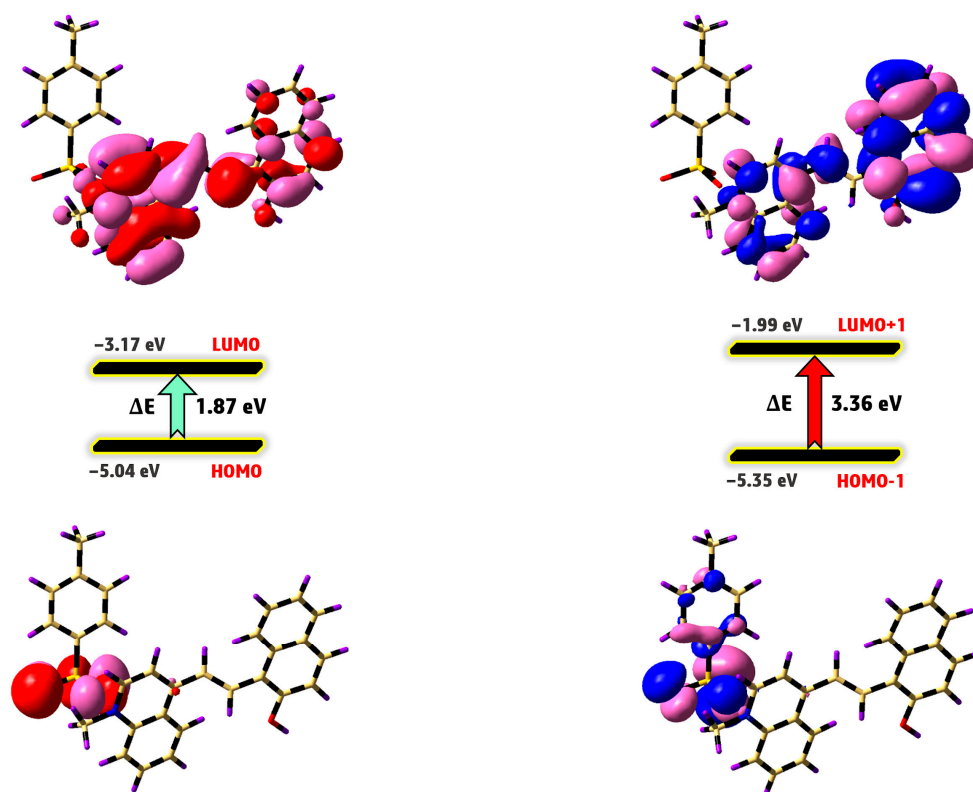


Figure 5. The distributions and energy surfaces of the molecular orbitals of SQ.

In addition to fundamental calculations, a deeper quantum chemical analysis was conducted to further elucidate the reactivity of the compound. The key descriptors were evaluated, including absolute hardness ($\eta = (E_{\text{LUMO}} - E_{\text{HOMO}})/2$), which reflects the compound's resistance to charge transfer, and absolute softness ($\sigma = 1/\eta$), indicating its adaptability to electronic changes. This study also computed the absolute electronegativity ($\chi = -(E_{\text{HOMO}} + E_{\text{LUMO}})/2$), which describes the compound's affinity for electrons, as well as the chemical potential ($P_i = -\chi$), representing the compound's tendency to release or accept electrons. Additional values, such as the additional electronic charge ($\Delta N = -P_i/\eta$) and global electrophilicity ($\omega = P_i^2/2\eta$), which gauge its propensity to interact with electron-rich species, were calculated to provide a comprehensive view of the SQ compound's reactivity characteristics. The values of P_i , ω , η , χ , σ , and ΔN for SQ are calculated to be −4.10 eV, 9.03 eV, 0.93 eV, 4.10 eV, 1.07 eV^{−1}, and 4.41, respectively. In the synthesized compound, the P_i parameter is consistently negative, indicating that its structure remains stable and does not break down into fundamental elements. The ω value suggests that this compound is capable of forming multiple binding modes with biological macromolecules [45], potentially enhancing its inhibitory effects. Additionally, the SQ compound shows a low absolute hardness of 0.93 eV, highlighting its increased reactivity.

3.3. In Silico Calculations

The compound's drug-likeness and ADMET characteristics have also been theoretically predicted using an in silico approach. When this non-covalent contact is included in the

drug design, it causes the conformational restriction of tiny drug molecules, which results in increased pharmacological activity, lipophilicity, and membrane permeability [46,47].

To be deemed a potential drug candidate, a molecule must fulfill three requirements: it must enter the body, reach its pharmacological target, accumulate sufficient concentration at the target site, and remain in active form for an extended period of time to demonstrate the expected biological activity. Several substances failed as medicines due to their limited bioavailability and poor pharmacokinetics.

PASS Online predicted the anti-inflammatory and antioxidant activity of 5.

The ADME profile of the SQ was clarified using the SwissADME web tools (Table 1). Eight physicochemical characteristics, including the four factors outlined in Lipinski's "rule of five", are used to measure a compound's drug-likeness [48–50]. A molecular weight less than 500 g/mol, XLOGP3 (−0.7 to +5.0), topological polar surface area between 130 Å², predicted solubility not exceeding 6, and flexibility or rotatable bonds not exceeding 9 are some of the requirements.

Table 1. ADME parameters of the SQ (5) representing drug-likeness.

Compound	MW, g/mol	XLOGP3	ESOL Log S	TPSA, Å ²	RB	BA	SA	LD ₅₀ , mg/kg
5	483.58	6.60	−7.35	107.41	3	0.55	3.22	5000

MW: Molecular weight; XLOGP3: octanol/water partition coefficient; ESOL LogS: estimated aqueous solubility; TPSA: topological polar surface area; RB: rotatable bonds; BA: bioavailability; SA: synthetic accessibility; predicted LD₅₀: lethal dose to 50% of animals.

The synthesized SQ salt satisfied the standard values of the drug-likeness notion by having three rotatable bonds, a molecular weight of 483.58 g/mol, and a TPSA of 107.41 Å². Good oral absorption was associated with the compound's bioavailability score of 0.55 [51]. It also has an excellent synthetic accessibility score of 3.22, which is a crucial factor in the process of finding new drugs. Cytochrome P450 (CYP) inhibition results in pharmacological toxicity [52,53]. The named molecule is not anticipated to inhibit the CYP1A2, CYP2C9, CYP2C19, CYP2D6, or CYP3A4 isoforms, according to the calculations. With a log Kp of −4.62, the compound demonstrated good skin permeability. The SQ's toxicity falls into the safer zone (toxicity class: 5), according to acute toxicity data (ProTox-II). Since the compound's calculated LD₅₀ was 5000 mg/kg, it can be regarded as nearly non-toxic. While there was no evidence of other organ toxicities, immunotoxicity was expected to be present (0.71% chance).

To confirm the predicted biological activities, the compound was assessed in vitro for its antioxidant capacity and in vitro/ex vivo for its anti-inflammatory potential.

3.4. Anti-Inflammatory Potential

3.4.1. Inhibition of Albumin Denaturation

Inflammation is a complex defense mechanism of the body that fights off dangerous microbes or damaged cells [54,55]. Nonetheless, this response needs to be controlled to avoid the development of clinical disorders linked to the immune system [3]. Disorders of inflammation are the body's response to tissue damage. The body is more vulnerable to the development of cancer, neurological illnesses, and autoimmune diseases when unchecked acute inflammation leads to chronic inflammation [56,57]. Conversely, chronic inflammation is a long-term response that is characterized by a gradual alteration in the cells that are present at the site of inflammation [57,58]. The immune response involves the nuclear factor-kappa B signaling pathway. It is essential to inflammatory processes due to its involvement in the transcription of cytokines such as nitric oxide (NO), interleukin-1β (IL-1β), tumor necrosis factor-α (TNF-α), and interleukin-6 (IL-6). Substances that

can disrupt this route are of interest to the pharmaceutical sector [59–61]. Patients with inflammatory illnesses are most frequently prescribed glucocorticoids or nonsteroidal anti-inflammatory drugs. The severe adverse effects of these drugs, like bleeding and stomach ulcers, have decreased their therapeutic effectiveness and usually lead to patients stopping their therapy [62]. In this context, the pharmaceutical industry has focused its efforts on finding novel bioactive compounds that have fewer adverse effects and superior therapeutic outcomes.

Based on its structure, the *in silico* calculations predicted the anti-inflammatory potential of SQ (5). Therefore, the main goal of this research was to establish the anti-inflammatory potential of SQ. *In vitro* antidenaturation of albumin was used to evaluate its anti-inflammatory properties. The obtained data showed that the IC₅₀ of the compound was 350 µg/mL, while the IC₅₀ of diclofenac was 471.3 µg/mL, which confirms a better anti-inflammatory effect of SQ (5). We can assume that the better anti-inflammatory effect of SQ is also due to the presence of a sulfonate group in the tosylate counterion [63,64].

3.4.2. Immunohistochemical Analysis

As one of the eleven members of the cytokine family, IL1 is mainly produced by the majority of immune cells in reaction to other cytokines or microbial stimuli [65]. Since IL-1 β plays a part in both autoimmune and inflammatory diseases, it is crucial to inhibit its activity in order to lower the inflammatory response. In necrotizing enterocolitis and inflammatory bowel disease, IL-1 β and other proinflammatory cytokines are increased, causing intestinal inflammation via breaking down the intestinal barrier [66]. This causes inflammation in the intestine. Furthermore, through regulating neuro-immune interactions across neuronal ganglia in the central nervous system, spinal cord, and digestive tract, IL-1 β is essential for the development and maintenance of neuropathic pain in a range of chronic illnesses [67]. Inflammation is one of the adaptive responses to a variety of traumas, including those caused by physical, chemical, and biological agents [68]. IL-1 β can cure acute inflammation and activate adaptive anti-tumor responses. Chronic inflammation, however, increases the risk of cancer [69]. Along with phenotypic changes in B and T cells, the production of cytokines through processes mediated by lipotoxicity and macrophage infiltration into adipose tissue, chronic and low-grade inflammation is the foundation of metabolic disorders [70,71]. Pro-inflammatory cytokines such as TNF- α , IL-8, and IL-2 are signs of intestinal dysbiosis. TH1 cells and macrophages produce the pro-inflammatory cytokines IFN- γ , IL-2, IL-3, and TNF, which can be blocked by the anti-inflammatory cytokine IL-10 [72]. On the other hand, cytokine IL-1 β directly affects the SMs and neurons in the stomach [73]. The innate immune system produces the potent pro-inflammatory cytokine IL-1 β . Unlike the usual method, it secretes proteins through one or more unconventional secretion pathways and is manufactured without the need for a signal sequence.

The immunohistological expression of IL-1 β in smooth muscle preparations (SMPs) incubated with SQ (5) was utilized in a semiquantitative manner (Figure 6, Table 2).

Table 2. Expression of IL-1 β and SQ's response.

	Control	SQ's Response
IL-1 β	++	+/-
SM	++	+/-
MP	++	—

SM and neurons in the MP were shown to express IL-1 β on a panel. By measuring the expression of IL-1 β in tissue slices using immunohistochemical staining, the semiquantitative method for reporting its expression was established. ++, moderate; +, low; —, absent.

Any histological changes between the SQ-incubated preparations stained with H-E and the control were noted (Figure 6B). Weak IL-1 β expression was observed in the MP in control preparations (Figure 6C). The preparations incubated with SQ (5) in the MP showed no expression of IL-1 β , with only a tiny percentage of SM cells labeled with IL-1 β (Figure 6D).

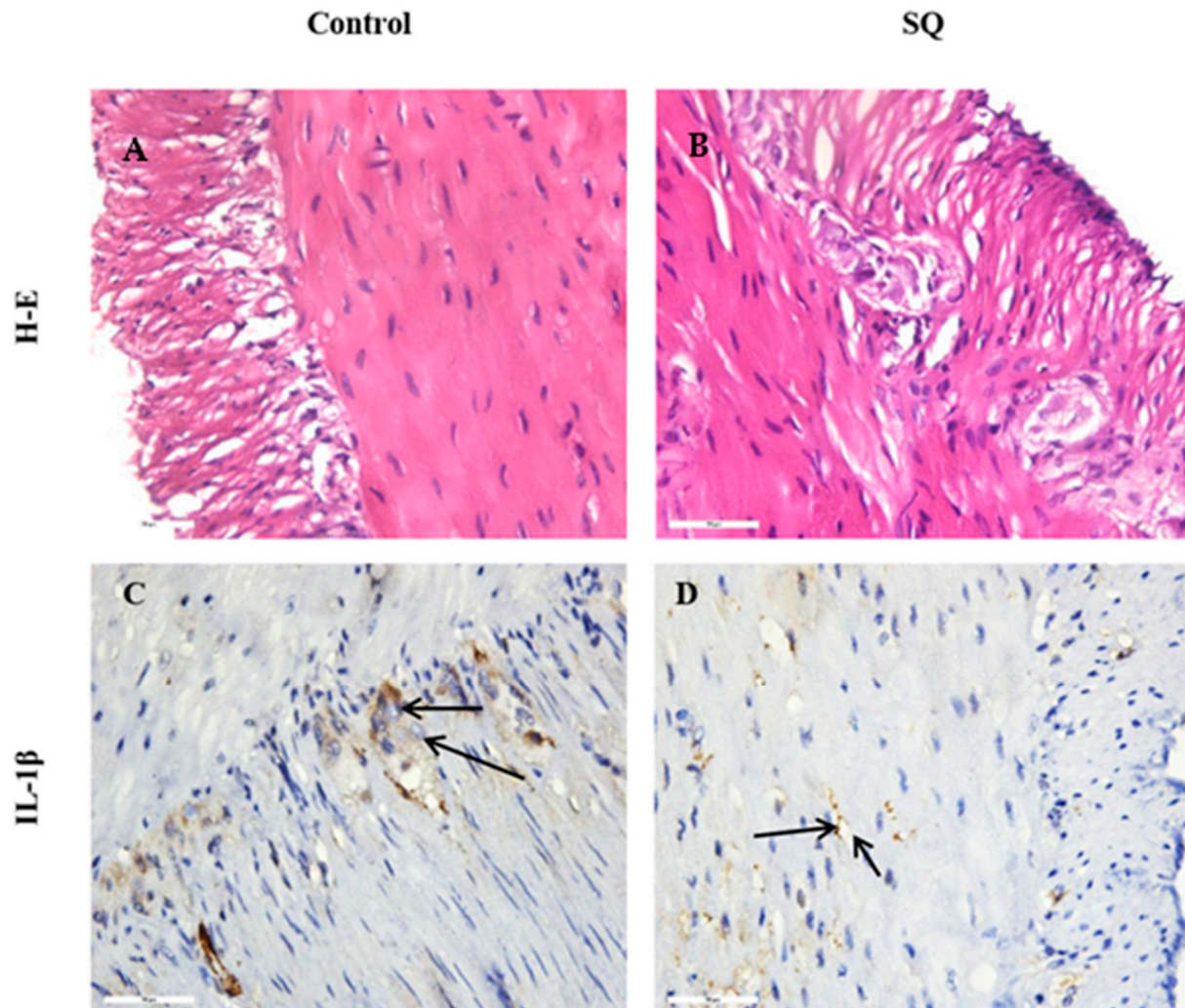


Figure 6. Representative histological micrographs of SM cells and myenteric ganglia from the rat's stomach corpus after 3 h incubation period. (A) Control, stained with H-E ($\times 400$); (B) preparations incubated with SQ, stained with H-E ($\times 400$); (C) control, with weak expression of IL-1 β in the myenteric plexus (MP, black arrows); (D) preparations incubated with SQ with no expression of IL-1 β expression in the MP (black arrows) ($\times 400$).

We found that both SM and MP neurons showed the anti-inflammatory activity of SQ, which we observed as reduced or absent IL-1 β expression in preparations. This suggests that the SQ might be able to lessen inflammatory processes in many somatic constituents of cells. For this reason, SQ may be able to reduce gastrointestinal tract inflammation [29]. Therefore, SQ (5) will be established as a potential medication to treat inflammatory illnesses through future preclinical experiments.

3.4.3. DPPH Radical Scavenging Activity

Finally, the DPPH radical scavenging assay [74] was used to assess the SQ's antioxidant capacity in vitro using rutin and quercetin as standards. At a dosage of $24 \pm 0.1 \mu\text{M}$, we found that the SQ (5) showed a 32% percentage inhibition, in contrast to the antioxidant

activity of rutin (40 μ M with 40% inhibition) and quercetin (20 μ M with 49% inhibition). The data obtained indicated that SQ (5) had lower antioxidant activity than quercetin but better than rutin.

3.5. Molecular Docking Simulation

Molecular docking simulation is a computational approach used to model interactions between macromolecules and smaller compounds, particularly highlighting the non-covalent biochemical interactions between them. This method enables a detailed visualization and assessment of these molecular interactions, providing valuable insights into potential binding affinities and interaction modes [75]. Additionally, in vitro findings on anti-inflammatory activity can be further correlated with the binding affinities and interaction patterns identified in docking studies. In this study, molecular docking of the SQ compound was conducted to investigate its binding affinity and interaction mode with HSA in order to elucidate its anti-inflammatory properties. HSA contains two primary drug-binding sites, known as Sudlow sites I and II. Docking simulations were performed at these sites using a grid box with the dimensions of $60 \times 70 \times 60$ Å. The results indicated a more favorable binding free energy (ΔG) at Sudlow site I compared to Sudlow site II, suggesting a stronger interaction of the SQ compound with Sudlow site I of HSA. Figure 7 shows the binding representation of the synthesized compound with HSA. The amino acid residues of HSA involved in the interaction with the SQ compound are represented as 3D and 2D diagrams in Figure 8. The ΔG value for this compound was calculated to be -8.18 kcal/mol, indicating a strong binding affinity. This high affinity suggests that the SQ compound has a significant inhibitory effect on HSA, supporting its potential as an effective inhibitor of this protein.

Moreover, the docking analysis revealed that the binding interactions between the title compound and HSA are significantly influenced by a combination of hydrogen bonding, van der Waals forces, hydrophobic interactions, and electrostatic attractions. This interplay of forces underscores the complexity and specificity of the binding process, highlighting how each interaction contributes to the stability and affinity of the compound within the HSA binding sites. The SQ compound forms a complex network of interactions with several key amino acid residues of HSA. It establishes two hydrogen bonds with residues LYS 195 and GLU 153, reinforcing stability. Additionally, the compound engages in three electrostatic attractions with LYS 195, GLU 292, and GLU 153, which further stabilize the binding. Hydrophobic interactions are prevalent, with five key connections to ARG 257, HIS 242, VAL 241, and ALA 291. Lastly, four van der Waals forces with residues ILE 290, LEU 260, LEU 238, and SER 192 contribute to the overall structural cohesion of the complex.

A high degree of interaction between the SQ (5) and amino acid residues within HSA plays a crucial role in stabilizing the albumin's structure. These interactions contribute to preserving the integrity of albumin, preventing its denaturation even under inflammatory conditions [76]. The results of this study align well with the observed experimental evidence of the compound's anti-inflammatory effectiveness, affirming its protective role during inflammation.

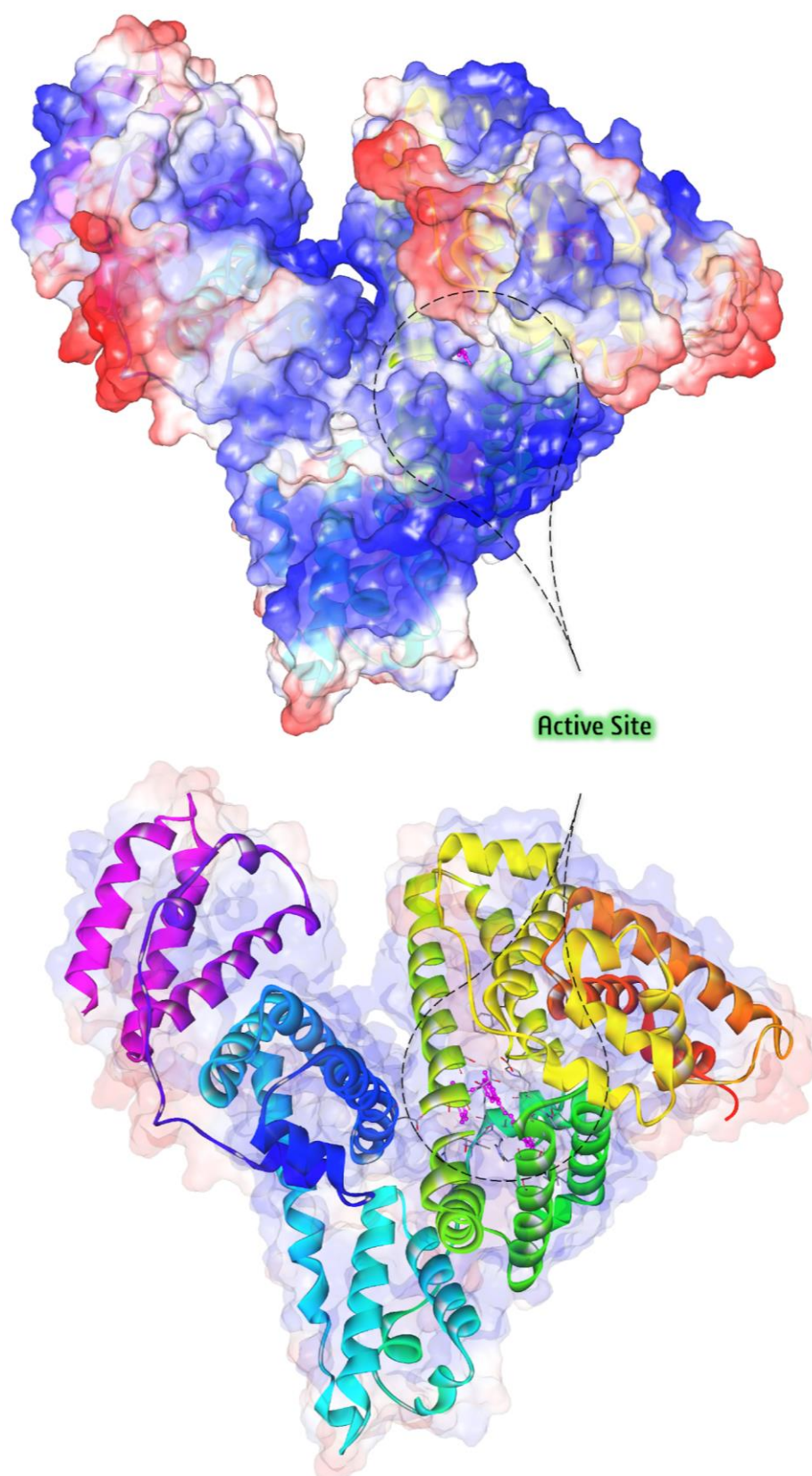


Figure 7. The docking perspective of SQ (5) in the interaction with HSA.

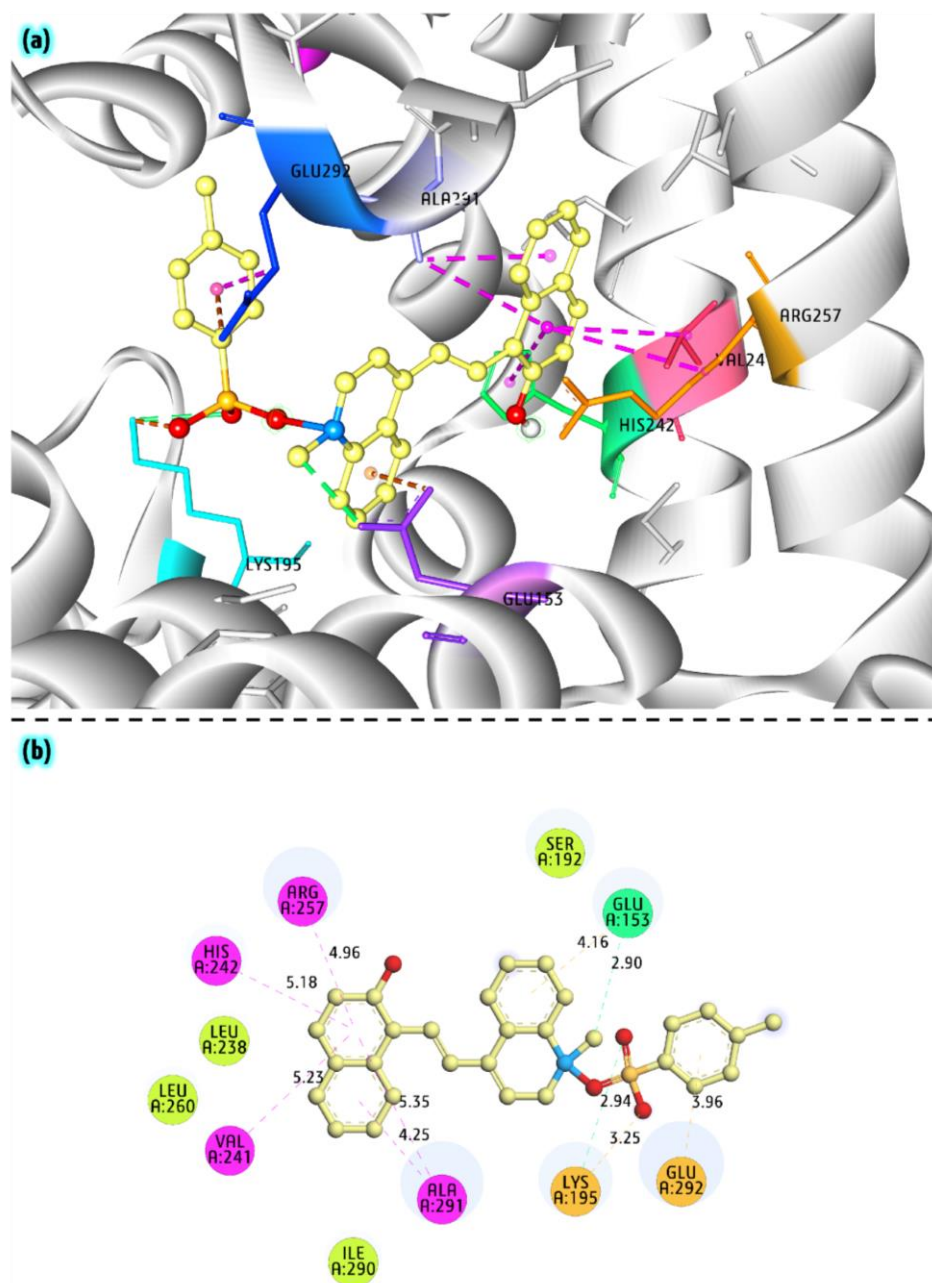


Figure 8. The 3D (a) and 2D (b) docking diagrams of SQ (5) in the interaction with HSA. The bond between oxygen and nitrogen is hypothetical. The purple, green, and orange dashed lines are the hydrophobic interactions, hydrogen bonds, and electrostatic attractions.

4. Conclusions

In conclusion, a new SQ salt was obtained as stilbene's analog. The compound was characterized using its NMR, IR, Raman, UV-Vis, and MS spectra. The SQ has been determined by in silico data as an orally active compound with high gastrointestinal absorption, anti-inflammatory, antioxidant activity and no toxic effect. The HOMO-LUMO analysis revealed that the electron density in the HOMO is concentrated primarily on the anionic SO_3^- group, while the LUMO's electron density is distributed across the cationic regions, suggesting an electron transfer pathway from the SO_3^- group to the cationic portions of the molecule. The biological evaluation results showed that SQ exhibits a preventive effect better than diclofenac on albumin denaturation. Furthermore, the ex vivo investigations assessing SQ's impact on IL-1 expression validated its anti-inflammatory capabilities. The DPPH radical scavenging data indicate that SQ exhibits lower antioxidant

activity than quercetin but better levels than rutin. Future preclinical experiments will therefore help to establish SQ as a viable therapeutic alternative for the treatment of inflammatory diseases. Furthermore, the docking simulation demonstrated that a high degree of interaction between the SQ compound and amino acid residues within HSA plays a crucial role in stabilizing the albumin's structure. Our future plans involve the synthesis of novel SQ derivatives with N,N-dimethylamino groups instead of hydroxyl groups in a naphthyl ring and longer alkyl groups attached to quaternary nitrogen, as well as a comparative study of their anti-inflammatory, antimicrobial, and antioxidant activity. Future in vivo and preclinical experiments will contribute to the establishment of these novel SQ derivatives as potential drug candidates.

Supplementary Materials: The following supporting information can be downloaded at: <https://www.mdpi.com/article/10.3390/app15010284/s1>, Figure S1: Electronic spectra of SQ, measured in acetonitrile, water, methanol, and chloroform at the same concentration of solutions, Figure S2: (A) Solid-state IR spectrum of SQ in the region of 4000–400 cm^{−1} measured in a KBr disc, (B) Raman spectrum of SQ in the region of 1800–400 cm^{−1}, Figure S3: ¹H NMR spectrum of SQ measured in DMSO d6 presented in the 9.4–6.0 ppm region, Figure S4: ¹H NMR spectrum of SQ measured in DMSO d6 presented in the 6.0–0 ppm region, Figure S5: ¹³C NMR spectrum of SQ measured in DMSO d6, Figure S6: COSY spectrum of SQ presented in the 9.4–7.0 ppm region, Figure S7: HSQC spectrum of SQ, Figure S8: HMBC spectrum of SQ in the region 9.7–6.7 ppm, Figure S9: HESI of SQ.

Author Contributions: Conceptualization, M.T., R.B. and T.K.; methodology, M.T. and R.B.; software, S.N., M.M., M.F.-D. and E.C.; formal analysis, M.T., R.B., M.P., K.S., G.M.Z. and P.N.; investigation, M.T., R.B., M.P., M.M., S.N., K.S., G.M.Z. and P.N.; writing—original draft preparation, S.N., M.M. and M.F.-D.; writing—review and editing, S.N., M.M., M.F.-D. and R.B.; visualization, M.T., M.P., R.B. and M.F.-D.; supervision, M.T. and S.N.; project administration, M.T. and S.N. All authors have read and agreed to the published version of the manuscript.

Funding: This research received no external funding.

Institutional Review Board Statement: This study was approved by the decision of the Ethical Committee of the Bulgarian Food Agency with No. 229/09.04.2019 and carried out following the guidelines of the European Directive 2010/63/EU. All experiments were conducted following the legislation on the Welfare and Protection of Animals Used for Experimental and Other Scientific Purposes.

Informed Consent Statement: Not applicable.

Data Availability Statement: The original contributions presented in the study are included in the article/Supplementary Materials, further inquiries can be directed to the corresponding author.

Acknowledgments: This study is part of Scientific Project BG-175467353-2023-13-0075-C01, No KP-06-H73/11 of the National Fund for Scientific Research in Bulgaria, National Program for Basic Research Projects—2023.

Conflicts of Interest: The authors declare no conflicts of interest.

References

1. Marchi, S.; Guilbaud, E.; Tait, S.W.; Yamazaki, T.; Galluzzi, L. Mitochondrial control of inflammation. *Nat. Rev. Immunol.* **2023**, *23*, 159–173. [CrossRef]
2. Nunes, C.D.R.; Barreto Arantes, M.; Menezes de Faria Pereira, S.; Leandro da Cruz, L.; de Souza Passos, M.; Pereira de Moraes, L.; Vieira, I.J.C.; Barros de Oliveira, D. Plants as Sources of Anti-Inflammatory Agents. *Molecules* **2020**, *25*, 3726. [CrossRef]
3. de Cássia da Silveira e Sá, R.; Andrade, L.N.; de Sousa, D.P. A review on anti-inflammatory activity of monoterpenes. *Molecules* **2013**, *18*, 1227–1254. [CrossRef]
4. Karpel, E. Mediatory ogólnoustrojowej odpowiedzi zapalnej—Znaczenie w praktyce klinicznej intensywnej terapii. *Anestezjol. Intensywna Ter.* **2001**, *3*, 181–190.
5. Li, Y.R.; Li, S.; Lin, C.-C. Effect of resveratrol and pterostilbene on aging and longevity. *Biofactors* **2018**, *1*, 69–82. [CrossRef]

6. Chan, E.W.C.; Wong, C.W.; Tan, Y.H.; Foo, J.P.Y.; Wong, S.K.; Chan, H.T. Resveratrol and pterostilbene: A comparative overview of their chemistry, biosynthesis, plant sources and pharmacological properties. *J. Appl. Pharm. Sci.* **2019**, *9*, 124–129. [[CrossRef](#)]
7. Artasensi, A.; Alessandro, P.; Vistoli, G.; Fumagalli, L. Type 2 diabetes mellitus: A review of multi-target drugs. *Molecules* **2020**, *25*, 1987. [[CrossRef](#)]
8. Choi, J.W.; Kim, G.J.; Kim, H.J.; Nam, J.-W.; Kim, J.; Chin, J.; Park, J.-H.; Choi, H.; Park, K.D. Identification and evaluation of a napyradiomycin as a potent Nrf2 activator: Anti-oxidative and anti-inflammatory activities. *Bioorg. Chem.* **2020**, *105*, 104434. [[CrossRef](#)]
9. Wu, P.-S.; Li, Y.-S.; Kuo, Y.-C.; Tsai, S.-J.J.; Lin, C.-C. Preparation and evaluation of novel transfersomes combined with the natural antioxidant resveratrol. *Molecules* **2019**, *24*, 600. [[CrossRef](#)]
10. Renaud, S.; de Lorgeril, M. Wine alcohol, platelets, and the French paradox for coronary heart disease. *Lancet* **1992**, *339*, 1523–1526. [[CrossRef](#)]
11. Keylor, M.H.; Matsuura, B.S.; Stephenson, C.R.J. Chemistry and biology of resveratrol-derived natural products. *Chem. Rev.* **2015**, *115*, 8976–9027. [[CrossRef](#)]
12. Akinwumi, B.C.; Bordun, K.M.; Anderson, H.D. Biological activities of stilbenoids. *Int. J. Mol. Sci.* **2018**, *19*, 792. [[CrossRef](#)]
13. Anisimova, N.Y.; Kiselevsky, M.V.; Sosnov, A.V.; Sadovnikov, S.V.; Stankov, I.N.; Gakh, A.A. *Trans*-, *cis*-, and dihydro-resveratrol: A comparative study. *Chem. Cen. J.* **2011**, *5*, 88. [[CrossRef](#)]
14. Orallo, F. Comparative studies of the antioxidant effects of *cis*- and *trans*-resveratrol. *Curr. Med. Chem.* **2006**, *13*, 87–98. [[CrossRef](#)]
15. Salehi, B.; Mishra, A.P.; Nigam, M.; Sener, B.; Kilic, M.; Sharifi-Rad, M.; Fokou, P.V.T.; Martins, N.; Sharifi-Rad, J. Resveratrol: A Double-Edged Sword in Health Benefits. *Biomedicines* **2018**, *63*, 91. [[CrossRef](#)]
16. Meng, X.; Zhou, J.; Zhao, C.N.; Gan, R.Y.; Li, H.B. Health Benefits and Molecular Mechanisms of Resveratrol: A Narrative Review. *Foods* **2020**, *9*, 340. [[CrossRef](#)]
17. Zhang, L.X.; Li, C.X.; Kakar, M.U.; Khan, M.S.; Wu, P.F.; Amir, R.M.; Dai, D.F.; Naveed, M.; Li, Q.Y.; Saeed, M.; et al. Resveratrol (RV): A pharmacological review and call for further research. *Biomed. Pharmacother.* **2021**, *143*, 112164. [[CrossRef](#)]
18. Hassan, M.; Abbasib, M.A.; Siddiqui, S.Z.; Shahzadi, S.; Raza, H.; Hussain, G.; Shah, S.A.A.; Ashraf, M.; Shahid, M.; Seo, S.Y.; et al. Designing of promising medicinal scaffolds for Alzheimer's disease through enzyme inhibition, lead optimization, molecular docking and dynamic simulation approaches. *Bioorg. Chem.* **2019**, *91*, 103138. [[CrossRef](#)] [[PubMed](#)]
19. Abdullah, M.A.; Lee, Y.-R.; Mastuki, S.T.; Leong, S.W.; Ibrahim, W.N.W.; Latif, M.A.M.; Ramli, A.N.M.; Aluwi, M.F.F.M.; Faudzia, S.M.M.; Kim, G.-H. Development of diarylpentadienone analogues as alpha-glucosidase inhibitor: Synthesis, *in vitro* biological and *in vivo* toxicity evaluations, and molecular docking analysis. *Bioorg. Chem.* **2020**, *104*, 104277. [[CrossRef](#)] [[PubMed](#)]
20. Mphahlele, M.J.; Gildenhuys, S.; Zamisa, S.J. Synthesis, Structure and Evaluation of the *N*-(2-Acetyl-4-(styryl)phenyl)-4-benzenesulfonamide Derivatives for Anticholinesterase and Antioxidant Activities. *Crystals* **2021**, *11*, 341. [[CrossRef](#)]
21. Banerjee, P.; Eckert, A.O.; Schrey, A.K.; Preissner, R. ProTox-II: A webserver for the prediction of toxicity of chemicals. *Nucleic Acids Res.* **2018**, *46*, W257–W263. [[CrossRef](#)] [[PubMed](#)]
22. Mazumder, K.; Hossain, E.; Aktar, A.; Mohiuddin, M.; Sarkar, K.K.; Biswas, B.; Aziz, A.; Abid, A.; Fukase, K. In Silico Analysis and Experimental Evaluation of Ester Prodrugs of Ketoprofen for Oral Delivery: With a View to Reduce Toxicity. *Processes* **2021**, *9*, 2221. [[CrossRef](#)]
23. Anzali, S.; Barnickel, G.; Cezanne, B.; Krug, M.; Filimonov, D.; Poroikov, V. Discriminating between Drugs and Nondrugs by Prediction of Activity Spectra for Substances (PASS). *J. Med. Chem.* **2001**, *44*, 2432–2437. [[CrossRef](#)] [[PubMed](#)]
24. Mathew, B.; Suresh, J.; Anbazhagan, S. Synthesis and PASS-assisted in silico approach of some novel 2-substituted benzimidazole bearing a pyrimidine-2,4,6 (trione) system as mucomembranous protector. *J. Pharm. Bioallied Sci.* **2013**, *5*, 39–43. [[CrossRef](#)] [[PubMed](#)]
25. Ekins, S.; Olechno, J.; Williams, A.J. Dispensing Processes Impact Apparent Biological Activity as Determined by Computational and Statistical Analyses. *PLoS ONE* **2013**, *8*, e62325. [[CrossRef](#)]
26. Milusheva, M.; Gledacheva, V.; Stefanova, I.; Feizi-Dehnyebi, M.; Mihaylova, R.; Nedialkov, P.; Cherneva, E.; Tumbarski, Y.; Tsoneva, S.; Todorova, M.; et al. Synthesis, Molecular Docking, and Biological Evaluation of Novel Anthranilic Acid Hybrid and Its Diamides as Antispasmodics. *Int. J. Mol. Sci.* **2023**, *24*, 13855. [[CrossRef](#)]
27. Milusheva, M.; Todorova, M.; Gledacheva, V.; Stefanova, I.; Feizi-Dehnyebi, M.; Pencheva, M.; Nedialkov, P.; Tumbarski, Y.; Yanakieva, V.; Tsoneva, S.; et al. Novel Anthranilic Acid Hybrids—An Alternative Weapon against Inflammatory Diseases. *Pharmaceuticals* **2023**, *16*, 1660. [[CrossRef](#)]
28. Docheva, M.; Dagnon, S.; Statkova-Abeghe, S. Flavonoid content and radical scavenging potential of extracts prepared from tobacco cultivars and waste. *Nat. Prod. Res.* **2014**, *28*, 1328–1334. [[CrossRef](#)] [[PubMed](#)]
29. Ricci, C.G.; Netz, P.A. Docking studies on DNA-ligand interactions: Building and application of a protocol to identify the binding mode. *J. Chem. Inf. Model.* **2009**, *49*, 1925–1935. [[CrossRef](#)] [[PubMed](#)]
30. Garrett, M.; Huey, R.; Lindstrom, W.; Sanner, M.F.; Belew, R.K.; Goodsell, D.S.; Olson, A.J. AutoDock4 and AutoDockTools4: Automated docking with selective receptor flexibility. *J. Comp. Chem.* **2009**, *30*, 2785–2791.

31. MGL Tools. 1.5. 6 (ADT)/MGL Tools 1. 6.; The Scripps Research Institute: La Jolla, CA, USA, 2016.
32. Dicle, S.; Kepekci, R.A.; Feizi-Dehneyebi, M.; Akkoc, S.; Cuevas-Vicario, J.V.; Micale, N. Biological Activities, DFT Calculations, and Molecular Docking Simulation of Thymol-Based Compounds. *Chem. Sel.* **2024**, *9*, e202304572. [\[CrossRef\]](#)
33. Mirshra, A.; Behera, R.K.; Behera, B.K.; Mishra, B.K.; Behera, G.B. Cyanines during the 1990s: A review. *Chem. Rev.* **2000**, *100*, 1973–2011. [\[CrossRef\]](#) [\[PubMed\]](#)
34. Tok, J.B.H.; Cho, J.; Rando, R.R. Aminoglycoside hybrids as potent RNA antagonists. *Tetrahedron* **1999**, *55*, 5741–5758. [\[CrossRef\]](#)
35. Hirano, M.; Osakada, K.; Nohira, H.; Miyashita, A. Crystal and solution structures of photochromic spirobenzothioiopyran. First full characterization of the meta-stable colored species. *J. Org. Chem.* **2002**, *67*, 533–540. [\[CrossRef\]](#) [\[PubMed\]](#)
36. Ivanova, B.; Kolev, T. Linearly polarized IR spectroscopy: Theory and applications for structural analysis. In *Effects in the Infrared Spectra of Crystals*; CRC Press, Taylor & Francis Group: Boca Raton, FL, USA; London, UK; New York, NY, USA, 2012; Volume Chapter 1, pp. 23–27.
37. Todorova, M.; Bakalska, R.; Kolev, T. Synthesis, crystal structure, and spectroscopic properties of new stilbazolium salt with enlarged π -conjugated system. *Spectrochim. Acta Part A Mol. Biomol. Spectrosc.* **2013**, *108*, 211–222. [\[CrossRef\]](#)
38. Kumar, M.K.; Sudhahar, S.; Bhagavannarayana, G.; Kumar, R.M. Crystal growth, spectral, structural and optical studies of π -conjugated stilbazolium crystal: 4-Bromobenzaldehyde-4'-N'-methylstilbazolium tosylate. *Spectrochim. Acta Part A Mol. Biomol. Spectrosc.* **2014**, *125*, 79–89. [\[CrossRef\]](#) [\[PubMed\]](#)
39. Politzer, P.; Murray, J.S. *Theoretical Biochemistry and Molecular Biophysics: A Comprehensive Survey*; Beveridge, D.L., Lavery, R., Eds.; Volume 2: Protein; Adenine Press: Schenectady, NY, USA, 1991.
40. Thul, P.; Gupta, V.P.; Ram, V.J.; Tandon, P. Structural and spectroscopic studies on 2-pyranones. *Spectrochim. Acta Part A Mol. Biomol. Spectrosc.* **2010**, *75*, 251–260. [\[CrossRef\]](#)
41. Mohammadi Ziarani, G.; Rezakhani, M.; Feizi-Dehneyebi, M.; Nikolova, S. Fumed-Si-Pr-Ald-Barb as a Fluorescent Chemosensor for the Hg^{2+} Detection and $\text{Cr}_2\text{O}_7^{2-}$ Ions: A Combined Experimental and Computational Perspective. *Molecules* **2024**, *29*, 4825. [\[CrossRef\]](#)
42. Panahande, Z.; Mohammadi Ziarani, G.; Feizi-Dehneyebi, M.; Badiei, A.; Abu-Dief, A.M. Synthesis and DFT Calculation of Hg^{2+} Fluorescence Chemosensor Based on a New Hybrid Organic–Inorganic Nanoporous Material of SBA-Pr-Is-Hy. *Appl. Organomet. Chem.* **2024**, e7818. [\[CrossRef\]](#)
43. Abu-Dief, A.M.; El-Khatib, R.M.; El-Dabea, T.; Feizi-Dehneyebi, M.; Barnawi, I.O.; Alsehli, A.H.; Al-Ghamdi, K.; El-Remaily, M.A.E.A.A. Design, preparation, physicochemical characterization, structural conformational, biological evaluation, and DNA interaction for some new benzimidazole complexes. *Appl. Organomet. Chem.* **2024**, *38*, e7358. [\[CrossRef\]](#)
44. Zahirović, A.; Fetahović, S.; Feizi-Dehneyebi, M.; Višnjevac, A.; Bešta-Gajević, R.; Kozarić, A.; Martić, L.; Topčagić, A.; Roca, S. Dual Antimicrobial-Anticancer Potential, Hydrolysis, and DNA/BSA binding affinity of a novel Water-Soluble Ruthenium-Arene ethylenediamine Schiff base (RAES) organometallic. *Spectrochim. Acta Part A Mol. Biomol. Spectrosc.* **2024**, *318*, 124528. [\[CrossRef\]](#)
45. Lanez, T.; Feizi-Dehneyebi, M.; Lanez, E. Assessment of the electrostatic binding of ferrocenylmethyl-nitroaniline derivatives to DNA: A combined experimental and theoretical study. *J. Mol. Struct.* **2024**, *1308*, 138386. [\[CrossRef\]](#)
46. Hayes, K.L.; Lasher, E.M.; Choczynski, J.M.; Crisci, R.R.; Wong, C.Y.; Dragonette, J.; Deschner, J.; Cardenas, A.J.P. Brooker's merocyanine: Comparison of single crystal structures. *J. Mol. Struct.* **2018**, *1161*, 194–198. [\[CrossRef\]](#)
47. Dado, G.P.; Gellman, S.H. Intramolecular hydrogen bonding in derivatives of beta-alanine and gamma-amino butyric acid; model studies for the folding of unnatural polypeptide backbones. *J. Am. Chem. Soc.* **1994**, *116*, 1054–1062. [\[CrossRef\]](#)
48. Daina, A.; Michielin, O.; Zoete, V. Swiss ADME: A free web tool to evaluate pharmacokinetics, drug-likeness and medicinal chemistry friendliness of small molecules. *Sci. Rep.* **2017**, *7*, 42717. [\[CrossRef\]](#)
49. Lipinski, C.A.; Lombardo, F.; Dominy, B.W.; Feeney, P.J. Experimental and computational approaches to estimate solubility and permeability in drug discovery and development settings. *Adv. Drug Deliv. Rev.* **2001**, *46*, 3–26. [\[CrossRef\]](#) [\[PubMed\]](#)
50. Bickerton, G.R.; Paolini, G.V.; Besnard, J.; Muresan, S.; Hopkins, A.L. Quantifying the chemical beauty of drugs. *Nat. Chem.* **2012**, *4*, 90–98. [\[CrossRef\]](#) [\[PubMed\]](#)
51. Martin, Y.C. A bioavailability score. *J. Med. Chem.* **2005**, *48*, 3164–3170. [\[CrossRef\]](#)
52. Kevin, B.; Robert, W.; Iain, G.; Kevin, D. Design of ester prodrugs to enhance oral absorption of poorly permeable compounds: Challenges to the discovery scientist. *Curr. Drug Metab.* **2003**, *4*, 461–485. [\[CrossRef\]](#)
53. Mishra, S.; Dahima, R. In vitro adme studies of TUG-891, a GPR-120 inhibitor using Swiss adme predictor. *J. Drug Deliv. Ther.* **2019**, *9*, 366–369. [\[CrossRef\]](#)
54. Ferrero-Miliani, L.; Nielsen, O.H.; Andersen, P.S.; Girardin, S.E. Chronic inflammation: Importance of NOD2 and NALP3 in interleukin-1 β generation. *Clin. Exp. Immunol.* **2007**, *147*, 227–235. [\[CrossRef\]](#) [\[PubMed\]](#)
55. Stone, M.J. Regulation of Chemokine–Receptor Interactions and Functions. *Int. J. Mol. Sci.* **2017**, *18*, 2415. [\[CrossRef\]](#)
56. Nizamutdinova, I.T.; Dusio, G.F.; Gasheva, O.Y.; Skoog, H.; Tobin, R.; Peddaboina, C.; Meininger, C.J.; Zawieja, D.C.; Newell-Rogers, M.K.; Gashev, A.A. Mast cells and histamine are triggering the NF- κ B-mediated reactions of adult and aged perilymphatic mesenteric tissues to acute inflammation. *Aging* **2016**, *8*, 3065–3090. [\[CrossRef\]](#) [\[PubMed\]](#)

57. Ejaz Ahmed, M.; Khan, M.M.; Javed, H.; Vaibhav, K.; Khan, A.; Tabassum, R.; Ashafaq, M.; Islam, F.; Safhi, M.M.; Islam, F. Amelioration of Cognitive Impairment and Neurodegeneration by Catechin Hydrate in Rat Model of Streptozotocin-Induced Experimental Dementia of Alzheimer's Type. *Neurochem. Int.* **2013**, *62*, 492–501. [\[CrossRef\]](#) [\[PubMed\]](#)
58. Kodydkova, J.; Vavrova, L.; Stankova, B.; Macasek, J.; Krechler, T.; Zak, A. Antioxidant Status and Oxidative Stress Markers in Pancreatic Cancer and Chronic Pancreatitis. *Pancreas* **2013**, *42*, 614–621. [\[CrossRef\]](#)
59. Wang, J.; Liu, Y.T.; Xiao, L.; Zhu, L.; Wang, Q.; Yan, T. Anti-inflammatory effects of apigenin in lipopolysaccharide-induced inflammatory in acute lung injury by suppressing COX-2 and NF- κ B pathway. *Inflammation* **2014**, *37*, 2085–2090. [\[CrossRef\]](#) [\[PubMed\]](#)
60. Polesso, F.; Sarker, M.; Anderson, A.; Parker, D.C.; Murray, S.E. Constitutive expression of NF- κ B inducing kinase in regulatory T cells impairs suppressive function and promotes instability and pro-inflammatory cytokine production. *Sci. Rep.* **2017**, *7*, 14779. [\[CrossRef\]](#) [\[PubMed\]](#)
61. Islam, S.S.; Al-Sharif, I.; Sultan, A.; Al-Mazrou, A.; Remmal, A.; Aboussekhra, A. Eugenol potentiates cisplatin anti-cancer activity through inhibition of ALDH-positive breast cancer stem cells and the NF- κ B signaling pathway. *Mol. Carcinog.* **2018**, *57*, 333–346. [\[CrossRef\]](#)
62. Bermas, B. Non-steroidal anti inflammatory drugs, glucocorticoids and disease modifying anti-rheumatic drugs for the management of rheumatoid arthritis before and during pregnancy. *Curr. Opin. Rheumatol.* **2014**, *26*, 334–340. [\[CrossRef\]](#)
63. Sun, Y.; Liu, Z.; Song, S.; Zhu, B.; Zhao, L.; Jiang, J.; Liu, N.; Wang, J.; Chen, X. Anti-inflammatory activity and structural identification of a sulfated polysaccharide CLGP4 from *Caulerpa lentillifera*. *Int. J. Biol. Macromol.* **2020**, *146*, 931–938. [\[CrossRef\]](#)
64. Lvhu, L.; Weifang, Z.; Lei, Y.; Ying, L.; Yanyan, Z. Ameliorative antibacterial, anti-inflammatory, and osteogenic activity of sulfonate-bearing polyetheretherketone toward orthopedic and dental implants. *Mater. Lett.* **2021**, *305*, 130774. [\[CrossRef\]](#)
65. McEntee, C.P.; Finlay, C.M.; Lavelle, E.C. Divergent Roles for the IL-1 Family in Gastrointestinal Homeostasis and Inflammation. *Front. Immunol.* **2019**, *10*, 1266. [\[CrossRef\]](#) [\[PubMed\]](#)
66. Kaminsky, L.W.; Al-Sadi, R.; Ma, T.Y. IL-1 β and the Intestinal Epithelial Tight Junction Barrier. *Front. Immunol.* **2021**, *12*, 767456. [\[CrossRef\]](#)
67. Ren, K.; Torres, R. Role of interleukin-1 β during pain and inflammation. *Brain Res. Rev.* **2009**, *60*, 57–64. [\[CrossRef\]](#) [\[PubMed\]](#)
68. Kaneko, N.; Kurata, M.; Yamamoto, T.; Morikawa, S.; Masumoto, J. The role of interleukin-1 in general pathology. *Inflamm. Regen.* **2019**, *39*, 1–16. [\[CrossRef\]](#)
69. Sell, H.; Habich, C.; Eckel, J. Adaptive Immunity in Obesity and Insulin Resistance. *Nat. Rev. Endocrinol.* **2012**, *8*, 709–716. [\[CrossRef\]](#)
70. Boulangé, C.L.; Neves, A.L.; Chilloux, J.; Nicholson, J.K.; Dumas, M.-E. Impact of the Gut Microbiota on Inflammation, Obesity, and Metabolic Disease. *Genome Med.* **2016**, *8*, 1–12. [\[CrossRef\]](#) [\[PubMed\]](#)
71. Acharya, A.; Thakur, S.; Muddapur, M. Evaluation of Serum Interleukin-10 Levels as a Predictor of Glycemic Alteration in Chronic Periodontitis and Type 2 Diabetes Mellitus. *J. Indian Soc. Periodontol.* **2015**, *19*, 388. [\[CrossRef\]](#)
72. Al Qudah, M.; Alfaqih, M.; Al-Shboul, O.; Saadeh, R.; Al-Dwairi, A. Effect of Cytokine Treatment on the Expression and Secretion of Brain Derived Neurotrophic Factor in the Smooth Muscle of the Rat Colon. *Biomed. Rep.* **2020**, *13*, 55–60. [\[CrossRef\]](#)
73. Xia, Y.; Hu, H.; Liu, S.; Ren, J.; Zafirov, D.H.; Wood, J.D. IL-1 β and IL-6 Excite Neurons and Suppress Nicotinic and Noradrenergic Neurotransmission in Guinea Pig Enteric Nervous System. *J. Clin. Investig.* **1999**, *103*, 1309–1316. [\[CrossRef\]](#)
74. Osman, N.I.; Sidik, N.J.; Awal, A.; Adam, N.A.; Rezali, N.I. In vitro xanthine oxidase and albumin denaturation inhibition assay of *Barringtonia racemosa* L. and total phenolic content analysis for potential anti-inflammatory use in gouty arthritis. *J. Intercult. Ethnopharmacol.* **2016**, *5*, 343–349. [\[CrossRef\]](#) [\[PubMed\]](#)
75. Isyaku, Y.; Uzairu, A.; Uba, S. Computational studies of a series of 2-substituted phenyl-2-oxo-, 2-hydroxyl- and 2-acyloxyethylsulfonamides as potent anti-fungal agents. *Heliyon* **2020**, *6*, e03724. [\[CrossRef\]](#)
76. Frisch, M.; Trucks, G.; Schlegel, H.B.; Scuseria, G.E.; Robb, M.A.; Cheeseman, J.R.; Scalmani, G.; Barone, V.; Mennucci, B.; Petersson, G. *Gaussian 09*, Revision D.01; Gaussian, Inc.: Wallingford, CT, USA, 2009; p. 201.

Disclaimer/Publisher's Note: The statements, opinions and data contained in all publications are solely those of the individual author(s) and contributor(s) and not of MDPI and/or the editor(s). MDPI and/or the editor(s) disclaim responsibility for any injury to people or property resulting from any ideas, methods, instructions or products referred to in the content.